SELF-SIMILAR SOLUTIONS FOR POROUS/PERFORATED WEDGE ENTRY PROBLEM

A. Iafrati, INSEAN (Italian Ship Model Basin),Italy,
A. A. Korobkin, Lavrentyev Institute of Hydrodynamics, Novosibirsk, Russia
E-mail: a.iafrati@insean.it,kaa@hydro.nsc.ru

1. INTRODUCTION

The flow generated by the water entry of a porous or perforated wedge is investigated. This activity is motivated by the wish of achieving a reduction in the hydrodynamic loads generated during the water impact of rigid and impermeable surfaces. The driving idea is to exploit such a reduction to improve ships' safety and comfort through the interposition of an intermediate thin layer between the rigid, impermeable, hull surface and the water. Other possible solutions consist in the interposition of a two-phase air-water layer, through blowing air beneath the ship hull.

The presence of an intermediate thin layer between the rigid contour and the water implies a modification in the boundary conditions on the surface of the entering body. Depending on the characteristics of the intermediate layer, different boundary conditions have to be enforced which relate the normal velocity at the external surface of the layer to that on the solid contour and to the pressure field. Simple relations occur in the case of porous and perforated layers. In the former case the liquid flow inside the layer is mainly driven by the balance between viscous losses and pressure gradient (Darcy's law). Hence, the boundary condition along the surface of the layer in contact with the liquid can be presented in the form:

$$V_{nL} = V_{nS} - \alpha_0 p \qquad (1)$$

where the coefficient α_0 characterizes the porosity of the layer, V_{nL} is the normal velocity on the surface of the layer and V_{nS} is the normal velocity on the surface of main structure, which is assumed rigid and impermeable. As $\alpha_0 \to 0$, the impermeable boundary condition is approached.

For a perforated surface, the flow through the layer is essentially governed by the balance between inertial terms and pressure gradients. In this case the condition is usually presented in the form (Molin and Korobkin, 2001)

$$V_{nL} = V_{nS} - \chi\sqrt{p/\varrho_w} \quad , \quad \chi^2 = \frac{2\mu\kappa^2}{1-\kappa} \ , \qquad (2)$$

μ being a discharge factor which is about 0.5, and κ the ratio between the area of the holes and the total area, ρ_w is the liquid density. As $\kappa \to 0$, the impermeable boundary condition is approached.

In order to clarify the effect of intermediate layer onto the pressure field and hydrodynamic loads, the water entry problem of a two-dimensional wedge is considered. The liquid is assumed ideal and incompressible, the liquid flow is symmetric and potential. The entry velocity V is constant. It is well-known that for a rigid impermeable wedge, the solution of the problem is self-similar once gravity and surface tension effects are neglected. Within the same assumptions, the flows generated by entry of porous or perforated wedge are still self-similar. The role of the corresponding non-dimensional parameters α and χ, where $\alpha = \alpha_0 V \varrho_w$, in terms of reduction of the total hydrodynamic load and of the pressure peak is evaluated.

In the following, the self-similar problem is formulated and the numerical method adopted for its solution is presented. As the free surface shape and the velocity potential on it, as well as the hydrodynamic pressure in the body boundary conditions (1) and (2), are unknowns, the solution is achieved via an iterative approach. At each iteration the boundary value problem is solved through a boundary element method. As a result of the flow singularity a thin jet layer develops along the body contour. The description of the flow within this thin layer is significantly simplified by the use of a shallow water approximation which is coupled with the boundary element approach used in the bulk of the fluid domain. Results are presented in terms of free surface shape, pressure distribution along the contour and total hydrodynamic load. As a preliminary validation step, solutions for a rigid and impermeable wedge are derived and comparisons with those available in literature are established.

2. FORMULATION OF THE PROBLEM

The self-similar solution for the water entry of a two-dimensional rigid and impermeable wedge has been analytically formulated by Dobrovol'skaya (1969) in the form of a rather complicated nonlinear, singular, integral equation in terms of the free surface slope. Owing to the behavior of the slope function at the jet tip, a very fine discretization and a quite sophisticated iterative procedure are needed to solve the problem, as shown by Zhao and Faltinsen (1993). Furthermore, in Dobrovol'skaya (1969) the problem has been formulated in terms of the Wagner function which significantly simplify the shape of the fluid domain in the case of a rigid and impermeable body surface. The same approach cannot be easily extended to the case of a porous/perforated body contour.

Hence, in the following, the similarity solutions is derived with the help of a different formulation. In terms of self-similar variables (Figure 1)

$$\xi = \frac{x}{Vt} \qquad \eta = \frac{y}{Vt} \qquad \phi = \frac{\varphi}{V^2 t} \ , \qquad (3)$$

the boundary value problem governing the self-similar so-

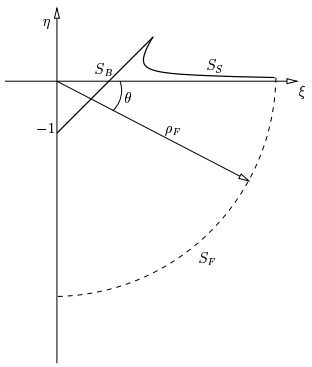

Figure 1: Sketch of the problem in self-similar variables. Due to the symmetry about the $x = 0$ axis, only the right hand side is shown.

lution about a porous/perforated wedge reads

$$\begin{aligned} \phi_{\xi\xi} + \phi_{\eta\eta} &= 0 && \text{in} && \Omega \\ \phi_n &= \cos\gamma - f(p) && \text{on} && S_B \\ \phi + \tfrac{1}{2}|\nabla\phi|^2 &= \xi\phi_\xi + \eta\phi_\eta && \text{on} && S_S \\ \nabla\phi \cdot \nabla H &= \xi H_\xi + \eta H_\eta && \text{on} && S_S \\ \phi(\xi,\eta) &= O(1/\rho) && \text{for} && \rho \to \infty \ . \end{aligned} \tag{4}$$

Equation $H(\xi,\eta) = 0$ describes the position of the free surface S_S, Ω denotes the fluid domain and S_B is the wetted part of the body surface. The normal to the body contour $\boldsymbol{n}$ is assumed to be oriented inside the fluid domain, so that $\boldsymbol{n} = (\sin\gamma, -\cos\gamma)$, γ being the deadrise angle of the wedge. The presence of a porous or perforated layer is represented by the function $f(p)$. The pressure p is nondimensionalized by the product $\varrho_w V^2$, where ϱ_w is the liquid density. For porous wedge $f(p) = \alpha p$ and for perforated wedge $f(p) = \chi\sqrt{p}$. The intermediate porous/perforated layer is assumed very thin, this is why the body boundary conditions are imposed on the surface of the main structure, $\eta = \xi\tan\gamma - 1$.

Although the above system of equation is independent of time its solution is still complicated because the boundary conditions on the free surface are strongly nonlinear and the free surface shape itself is unknown and has to be determined as a part of the solution. A significant simplification of the problem can be achieved by introducing a modified velocity potential $S(\xi,\eta)$

$$S(\xi,\eta) = \phi(\xi,\eta) - \frac{1}{2}\rho^2 \ , \tag{5}$$

which satisfy the Poisson equation $\nabla^2 S = -2$. From this definition the body boundary condition

$$\phi_\eta = \phi_\xi \tan\gamma - 1 + \frac{1}{\cos\gamma} f(p) \ ,$$

can be recast in the form

$$S_\eta = S_\xi \tan\gamma + \frac{1}{\cos\gamma} f(p) \quad \Rightarrow \quad S_n = -f(p) \ . \tag{6}$$

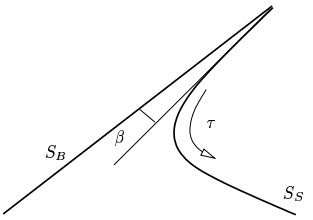

Figure 2: Sketch of the free surface configuration about the jet tip: τ is the curvilinear coordinate along the free surface with $\tau = 0$ at the jet tip.

It can be shown that the kinematic and dynamic boundary conditions on the free surface provide

$$S_n = 0 \ , \quad S + \frac{1}{2} S_\tau^2 = 0 \ . \tag{7}$$

In the above equations, τ is the parameter along the free surface which is assumed to be zero at the intersection point between the body contour and the free surface (Figure 2). Finally, in terms of S, the far field condition reads

$$S(\xi,\eta) \to -\frac{1}{2}\rho^2 \qquad \text{as} \quad \rho \to \infty \ . \tag{8}$$

The main advantage in using the modified velocity potential is that the dynamic boundary condition on the free surface can be integrated analytically, thus yielding

$$S(\tau) = -\frac{1}{2}\tau^2 \ . \tag{9}$$

The similarity solution is obtained with the help of a pseudo-time iterative procedure. A first guess for the free surface shape is assigned and, starting from the intersection point with the body contour, the curvilinear abscissa τ is initialized. In the body boundary condition the pressure is set zero at the first step of the iterative procedure. The boundary value problem

$$\begin{aligned} \nabla\phi &= 0 && \text{in} && \Omega \\ \phi_n &= \cos\gamma - f(p) && \text{on} && S_B \\ \phi &= \tfrac{1}{2}(\rho^2 - \tau^2) && \text{on} && S_S \\ \phi &\to 0 && \text{as } \rho \to \infty \ , \end{aligned} \tag{10}$$

is solved through a boundary integral representation of the velocity potential, thus providing the velocity potential along the body surface S_B and its normal derivative on the free surface. From the former, the pressure distribution along the body contour is updated as

$$p = -\phi + \phi_\tau \left(\xi\cos\gamma + \eta\sin\gamma\right) + \phi_n \cos\gamma - \frac{1}{2}\left[\phi_\tau^2 + \phi_n^2\right] \ , \tag{11}$$

while the normal derivative of the velocity potential along the free surface with the help of equation (5) provides S_n as

$$S_n = \phi_n - \boldsymbol{\rho} \cdot \boldsymbol{n} \ .$$

Then we check if the kinematic condition $S_n = 0$ is satisfied along the free surface. If this is not the case, the

free surface configuration is updated, the velocity potential along it is reinitialized and the boundary condition along the body contour is updated by using the new pressure distribution. After that the boundary value problem (10) is solved once again and the iterative procedure is repeated until convergence is achieved.

3. NUMERICAL MODEL

The boundary value problem (10) is numerically solved through a boundary integral representation of the velocity potential which gives the velocity potential at any point P of the fluid boundary. In the far field, the velocity potential is approximated with a dipole solution intensity of which, C_D, is unknown and is derived together with the solution of the boundary value problem. The boundary of the fluid domain is discretized with straight line panels along which a piecewise distribution for the velocity potential and for its normal derivative is assumed. By exploiting the symmetry with respect to the $\xi = 0$ axis, only the right hand side of the fluid domain is discretized and the image contribution is accounted for when evaluating the influence coefficients.

Once the boundary value problem (10) is solved, both the tangential and the normal velocity components are evaluated along the body contour and the free surface. The former are used to obtain the pressure distribution along the body surface. The latter are used to update the free surface shape in a time stepping fashion using $\nabla S = \nabla\phi - \boldsymbol{\rho}$ as a pseudo-velocity field (see Iafrati and Korobkin, 2004).

From the numerical point of view, a second order Runge-Kutta method is used for integration in time of the motion of the panel centroids. For stability reasons, the time step is chosen so that the product of the velocity by the time step is always smaller than one fourth of the corresponding panel size. At each iteration the distribution of the free surface panels is reinitialized with the new panel vertices located along a cubic spline curve passing through the centroids. The velocity potential along the free surface is also reinitialized at each iteration and the matching with the dipole solution is enforced in the far field.

Owing to the flow singularity at the intersection, a jet develops along the body contour. For small deadrise angles this jet is so thin that accurate description of the flow inside the jet cannot be easily achieved with boundary element approaches. Hence, a shallow water model similar to that adopted in Battistin and Iafrati (2004) is developed and coupled with the boundary element solver. The shallow water model is activated when the angle between the free surface and the body contour drops below a threshold value. When the model is activated, the thinnest part of the jet layer is removed from the boundary element representation and the shallow water solution provides a known contribution.

4. NUMERICAL RESULTS

Numerical simulations have been done for the rigid (impermeable) wedge with $\gamma = 10, 20, 30$ and 60 degrees and comparisons are established with results obtained by Zhao and Faltinsen (1993) through the Dobrovol'skaya's model (DOB) and the fully nonlinear numerical approach (NUM). Comparisons, reported in Tables 1-4, are established in terms of the vertical coordinate of the jet tip η_B, the maximum pressure coefficient $C_{p_{max}}$, the vertical coordinate of the pressure peak location y_{max} and the total, nondimensional, vertical force acting on the wedge, $F/(\varrho_w V^3 t)$. Comparisons indicate that the present method is rather reliable and accurate both in term of free surface shape and pressure distribution.

γ	ZF (DOB)	Present
10	2.1004	2.0971
20	1.9955	1.9920
30	1.8363	1.8278
60	1.0848	1.0822

Table 1: Vertical coordinate of the jet tip η_B.

γ	ZF (DOB)	ZF (BEM)	Present
10	77.847	80.200	77.661
20	17.774	18.200	17.727
30	6.927	6.940	6.883

Table 2: Pressure peak $p_{max}/(\varrho_w V^2)$.

γ	ZF (DOB)	ZF (BEM)	Present
10	0.5556	0.555	0.5549
20	0.5087	0.488	0.5080
30	0.4243	0.400	0.4229

Table 3: Pressure peak location y_{max}.

γ	ZF (DOB)	ZF (BEM)	Present
10	213.980	220.8	209.329
20	42.485	43.0	42.160
30	14.139	13.9	13.962

Table 4: Vertical hydrodynamic load $F/(\varrho_w V^3 t)$.

After the validation, the self-similar solutions characterizing the water entry flow about porous and perforated layers are investigated. Calculations are carried out for a wedge with deadrise angle $\gamma = 30$ degrees and the governing parameters α and χ being equal to $0.02, 0.05, 0.1, 0.2, 0.3, 0.4, 0.5$. For the perforated surface those values of χ correspond to hole area ratios $\kappa = 0.0199, 0.0493, 0.0976, 0.1910, 0.2809, 0.3679, 0.4529$. The behaviour of the most relevant quantities is reported in Tables 5 and 6. In both cases, an increase of α or χ reduces the pressure peak, the wetted length and the total hydrodynamic load. These features can be seen from Figure 3 and 4.

α	$C_{p_{max}}$	y_{max}	η_B	$F/(\varrho_w V^3 t)$
0.00	6.882740	0.422905719	1.827831	13.9625087
0.02	6.593664	0.405187994	1.775493	12.9453171
0.05	6.203160	0.380712384	1.704327	11.6086952
0.10	5.681808	0.345140679	1.604201	9.9821119
0.20	4.877164	0.288795334	1.457262	7.6923284
0.30	4.284656	0.244194449	1.354996	6.2128531
0.40	3.825980	0.215028445	1.280468	5.1779648
0.50	3.454216	0.185550673	1.222982	4.4649639

Table 5: Behavior of the most relavant quantities for increasing α in the case $\gamma = 30$.

χ	$C_{p_{max}}$	y_{max}	η_B	$F/(\varrho_w V^3 t)$
0.00	6.882740	0.422905719	1.827831	13.9625087
0.02	6.697824	0.409863377	1.796141	13.2888253
0.05	6.436386	0.398841182	1.745535	12.3562410
0.10	6.025650	0.369702315	1.667528	10.9096911
0.20	5.331568	0.312691862	1.530475	8.7011256
0.30	4.742064	0.268646388	1.416978	6.9656666
0.40	4.240086	0.228510729	1.323106	5.6041193
0.50	3.810718	0.195651993	1.245613	4.5751506

Table 6: Behavior of the most relavant quantities for increasing χ in the case $\gamma = 30$.

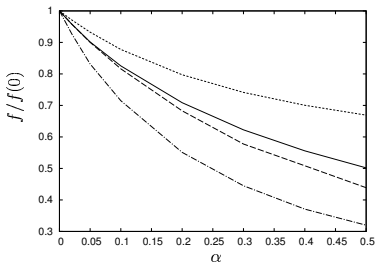

Figure 3: Behaviour of the quantities listed in Table 5 versus α. Quantities are divided by the corresponding value for $\alpha = 0$. $C_{p_{max}}$ solid, y_{max} dash, η_B dot, $F/(\varrho_w V^3 t)$ dash-dot.

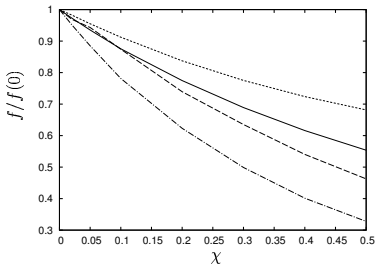

Figure 4: Behaviour of the quantities listed in Table 6 versus χ. Quantities are divided by the corresponding value for $\chi = 0$. $C_{p_{max}}$ solid, y_{max} dash, η_B dot, $F/(\varrho_w V^3 t)$ dash-dot.

It was revealed that the jet thickness vanishes when the permeability of the intermediate layer increases, thus making the description of the flow very challenging even for moderate deadrise angles. This aspect is shown in Figure 5, where the free surface profiles obtained for several α are drawn. In addition to the reduction of the jet thickness, a much sharper change in the slope occurs as the porous/perforated parameter is increased. Due to the very small thickness of the jet layer, the evaluation of the pressure field for relatively large values of α (or χ) is also very challenging and needs the development of different approaches. In Figure 6 the pressure distribution along the wetted part of the body are shown for porous layers. A rather uniform reduction of the pressure field is achieved, along with a contraction of the wetted area. As

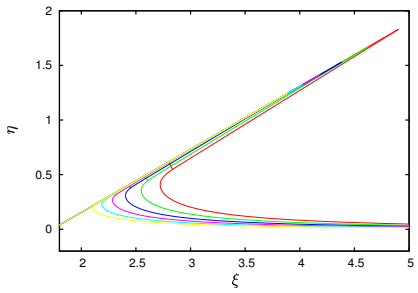

Figure 5: Effect of the porosity parameter α on the free surface shape: curves are drawn for $\alpha = 0, 0.1, 0.2, 0.3, 0.4, 0.5$.

indicated by the data listed in Tables 5 and 6, the location of the pressure peak moves toward the wedge apex.

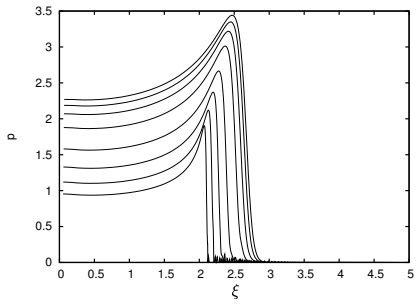

Figure 6: Effect of the porosity parameter α on the pressure distribution. Curves are drawn for $\alpha = 0, 0.1, 0.2, 0.3, 0.4, 0.5$.

Acknowledgements

This work has been done during the stay of A.I. at the Lavrentyev Institute of Hydrodynamics. The financial support provided by the Italian CNR NATO Fellowship (Bando N. 217.35 del 30/04/2003) is gratefully acknowledged.

References

Battistin D., Iafrati A. (2004) A numerical model for the jet flow generated by water impact, J. Engng. Math., **48**, 353-374.

Dobrovol'skaya, Z.N. (1969) On some problems of similarity flow of fluid with a free surface, J. Fluid Mech., **36**, 805-829.

Iafrati A., Korobkin A.A. (2004) Initial stage of flat plate impact onto liquid free surface, Physics of Fluids, **16**, 2214-2227.

Molin, B. & Korobkin, A.A. (2001) Water entry of a perforated wedge. In *16th IWWWFB* Proc. (Eds. K. Mori and H. Iwashita), Hiroshima 121-124.

Zhao R., Faltinsen O. (1993) Water entry of two-dimensional bodies, J. Fluid Mech., **246**, 593-612.